Decadal Variability of Pycnocline Flows from the Subtropical to the Equatorial Pacific*

QI WANG

Physical Oceanography Laboratory, Department of Marine Meteorology, Ocean University of China, Qingdao, China

RUI XIN HUANG

Department of Physical Oceanography, Woods Hole Oceanographic Institution, Woods Hole, Massachusetts

(Manuscript received 11 May 2004, in final form 21 December 2004)

ABSTRACT

A method based on isopycnal trajectory analysis is proposed to quantify the pathways from the subtropics to the Tropics. For a continuous stratified ocean a virtual streamfunction is defined, which can be used to characterize these pathways. This method is applied to the climatological dataset produced from a data-assimilated model. Analysis indicates that in each layer contours of the virtual streamfunction are a good approximation for streamlines, even if there is a cross-isopycnal mass flux. The zonal-integrated meridional transport per unit layer thickness through each pathway varies in proportion to $1/\sin\theta$, where θ is latitude. The vertical-integrated total transport through pathways behaves similarly. Transport through pathways has a prominent decadal variability. Results suggest that in decadal time scales the interior pathway transport (IPT) anomaly may be mainly caused by the wind stress anomaly at low latitude. The western boundary pathway transport (WBPT) anomaly often has a sign opposite to the IPT anomaly, reflecting compensation between the IPT and the WBPT. However, more often than not the wind stress anomaly within tropical latitudes can also be used to explain the WBPT anomaly.

1. Introduction

In the Pacific Ocean, subtropical water in the upper ocean is subducted into the thermocline and flows toward the equator, where it moves upward to surface layers and returns poleward, completing a cycle. This pathway of water has been called the subtropical cell (STC) (McCreary and Lu 1994). The STC is an important component of the global heat transport machinery (McCreary and Lu 1994; Rothstein et al. 1998). Tritium data collected from the oceans in the 1980s provide strong evidence for the existence of pycnocline flows from the subtropical North Pacific to the equator (Fine et al. 1987; McPhaden and Fine 1988). Subsequent modeling studies, including simple reduced-gravity models and ocean general circulation models (OGCMs), clearly demonstrate dynamical connection through this cell (McCreary and Lu 1994; Liu 1994; Liu et al. 1994; Lu and McCreary 1995; Lu et al. 1998; Liu and Huang 1998; Rothstein et al. 1998).

Meridional circulation associated with this cell is further divided into two components: the western boundary pathway (WBP) and the interior pathway (IP) (McCreary and Lu 1994; Liu et al. 1994; Rothstein et al. 1998). Corresponding pathways in the North (South) Pacific will be called NWBP and NIP (SWBP and SIP). These pathways and their variability on a decadal time scale have been discussed in previous studies. Johnson and McPhaden (1999) used historical CTD data to analyze IPs. Results from data-assimilated OGCM were discussed by Huang and Liu (1999). These studies reveal important dynamical aspects of these pathways, but many questions remain unanswered.

To better understand the communication between the Tropics and subtropics it is desirable to map out these pathways clearly. Huang and Wang (2001) postulated a simple index based on wind stress data. The

* Woods Hole Oceanographic Institution Contribution Number 11340.

Corresponding author address: Dr. Qi Wang, Department of Marine Meteorology, Ocean University of China, Qingdao 266003, China.
E-mail: wangqi@ouc.edu.cn

choke value of a virtual streamfunction, defined through the barotropic transport, was used to quantify the barotropic interior pathway. This was compared favorably to results obtained from a data-assimilated oceanic general circulation model.

In this study we will extend the same approach to baroclinic circulation in the Pacific Ocean, using three-dimensional velocity fields from the Simple Ocean Data Assimilation (SODA) dataset (Carton et al. 2000a,b). This paper is organized as follows. The data and method are described in section 2. Flows and pathways on different isopycnal surfaces are described in section 3. Transport through pathways is discussed in section 4. The innovative part of our study is the introduction of a virtual streamfunction for a continuously stratified ocean, discussed in section 5. This method is applied to the study of decadal variability of the tropical Pacific Ocean in section 6. Section 7 is the conclusion.

2. Data and method

The SODA dataset was generated from an oceanic general circulation model based on the Geophysical Fluid Dynamics Laboratory Modular Ocean Model MOM2.b code. The monthly analysis spans the period from January 1950 to December 2001. The domain of the model covers the global oceans within 60° of the equator, with $1° \times 1°$ horizontal resolution at mid latitudes and an enhanced resolution of $0.45 \times 1°$ at the Tropics. The model has 20 vertical levels on a stretched grid with 15-m high resolution near the surface and the center of the lowest grid at 3622.5 m. Assimilated data include temperature and salinity profiles from the *World Ocean Atlas-94* (MBT, XBT, CTD, and station data), as well as additional data of hydrography, sea surface temperature, and altimeter sea level. The data files include global temperature, salinity, and horizontal velocity (Carton et al. 2000a,b). To exclude the approximate contribution due to the ageostrophic flux associated with the Ekman transport, we will choose the interface at 45 m as the base of the Ekman layer and concentrate on analyzing data below 45 m.

A pathway can be identified by the first (last) trajectory at its eastern (western) edge. As long as the boundaries of the pathway are identified, there is no need to calculate individual trajectory. Flow trajectories on isopycnal surfaces are calculated from climatological (52 yr) mean velocity fields, starting from the edge of the equatorial region ($\pm 2.1°$) with a fourth-order Runge–Kutta backward time stepping. The IP consists of trajectories that can be traced back to the surface outcrop regimes or the high latitude western boundary, without passing the low latitude western boundary current (LLWBC). The WBP consists of trajectories that pass the LLWBC. The latitude bands identified as LLWBC are as follows: 6°–8°N for the North Pacific and 7°–4°S for the South Pacific. The width of the LLWBC is set to 3°. The "high latitudes" are defined as 20° off the equator.

3. Flow and pathways on isopycnal surfaces

Pathways from the Subtropical to the equatorial Pacific have been quantified at different isopycnal layers (Figs. 1a–d). The NIP (SIP) is located within density range $\sigma_\theta = 23.0$–26.2 kg m^{-3} ($\sigma_\theta = 23.0$–26.4 kg m^{-3}). The WBPs occupy a slightly larger range; however, we will focus primarily on the pycnocline range of $\sigma_\theta = 23.0$–26.4 kg m^{-3}.

In the North Pacific, water subducted in the central basin moves to the equatorial area through the NWBP. This water mass first flows southwestward after reaching the western boundary, turns southward, and then flows along the Mindanao Current (MC). After leaving the MC, some water (especially the upper-layer water) turns northeastward and flows along the North Equatorial Countercurrent (NECC), and finally joins the Equatorial Undercurrent (EUC) in the central basin; some water (especially water in deep layers) approaches the equator along the western boundary.

On the other hand, water subducted in the eastern basin is likely to feed the NIP. This water mass first flows southwestward within the North Equatorial Current (NEC), then turns eastward in the NECC, and finally converges into the EUC in the eastern basin. (In the upper layer a small amount of water reaches the equatorial region directly through a narrow passage in the eastern basin, as shown by gray lines in Figs. 1a and 1b.)

The NIP and NWBP are clearly separated at approximately 7°N in the western basin because of a small cyclonic gyre east of the Philippines (Huang and Wang 2001). In the eastern basin, there is also a cyclonic gyre generated by Ekman upwelling in the intertropical convergence zone (ITCZ). As a result, within this area surface layers are thin; thus, a high potential vorticity area exists, which is often called a "potential vorticity barrier" for the NIP (Lu and McCreary 1995). Local cyclonic circulation prevents a direct communication between the subtropics and Tropics.

On the other hand, it is difficult to find the latitude where the SWBP and SIP can be clearly separated; thus, we designate one boundary that serves as both the western boundary of the SIP and the eastern boundary of the SWBP. Water subduction in the central South

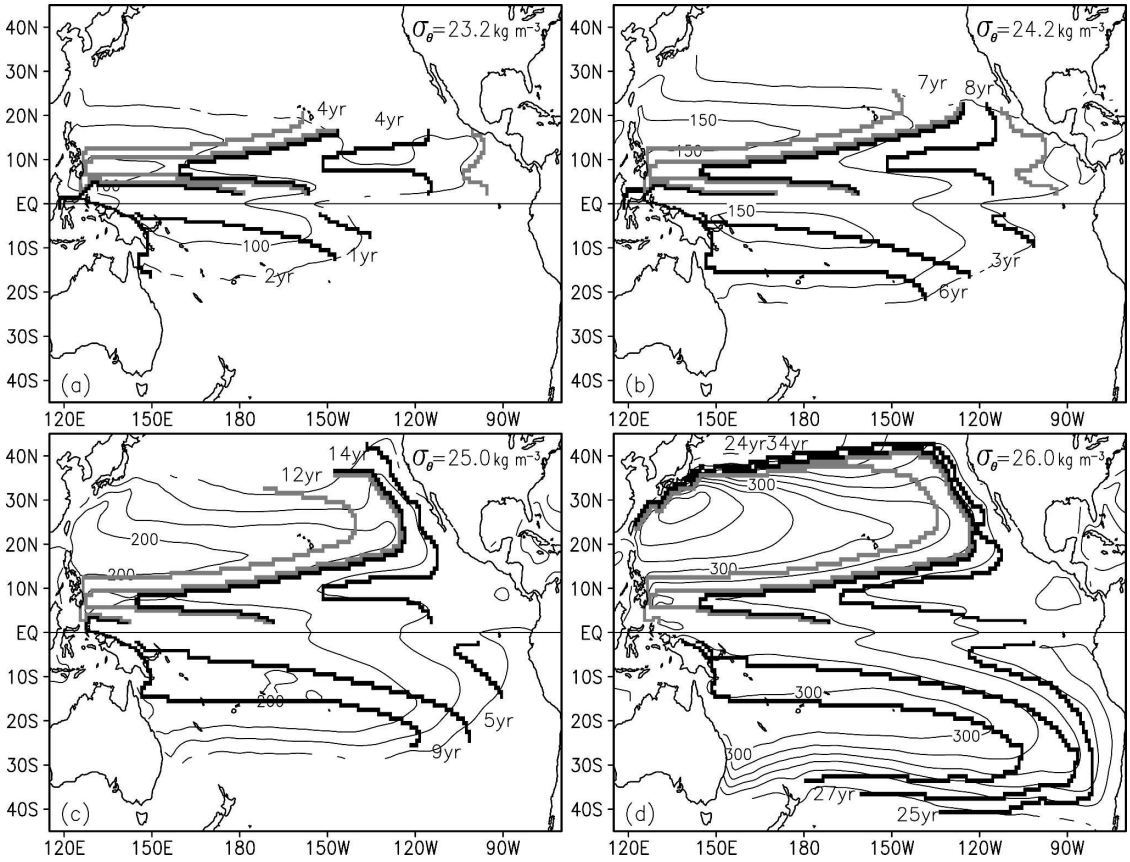

FIG. 1. Climatological-mean circulation on four isopycnal surfaces: σ_θ = (a) 23.2, (b) 24.2, (c) 25.0, and (d) 26.0 kg m^{-3}. Gray lines indicate depths (m); black and gray thick lines indicate pathways. The ventilation time for the pathways (yr) is indicated by a pair of numbers, the left for the western boundary pathway and the right for the interior pathway. Gray thick lines near the eastern boundary in (a) and (b) indicate a narrow local pathway, a shortcut, from the subtropics to the equatorial regime.

Pacific flows northwestward along the South Equatorial Current (SEC) and converges to the LLWBC. After crossing the equator, this water mass meets North Pacific water masses and turns eastward within the NECC. Eventually, it returns and joins the EUC. The SIP is straightforward: water subducted in the eastern extratropical basin flows northwestward within the SEC and hereafter joins the EUC directly.

The outcrop latitude of the pathway extends poleward with the increase of density. On the σ_θ = 26 kg m^{-3} surface, both the NIP and NWBP do not outcrop. In fact, water sources for these two pathways can be traced back to the California Current, the North Pacific Current, and Kuroshio.

The water sources of the EUC are indicated by pathways (Fig. 1). In the western basin Southern Hemisphere water through the SWBP is the main source because the SWBPs in most layers (apart from deep layers) cross the equator; in the central-western basin the SIP and NWBP are the main sources; and in the central-eastern basin, the NIP and SIP are the main sources. This is consistent with previous studies (Blanke and Raynaud 1997, their Fig. 10).

In the uppermost layers ($\sigma_\theta \leq$ 23.2 kg m^{-3}) the Indonesian Throughflow (ITF) is fed by the South Pacific LLWBC (Fig. 1a); for σ_θ = 23.4–25.0 kg m^{-3}, it is fed by the MC (Fig. 1b).

Ventilation time, defined as the average time for water to move through the pathway, increases with depth and it varies from a few years for shallow layers to more than 30 years for deep layers (Fig. 1).

4. Transports through pathways

The meridional volume transport within an isopycnal layer is

$$\mathrm{Tr}_n(\theta) = \int_{\phi Wn}^{\phi En} v_n(\phi, \theta) h_n(\phi, \theta) R \cos\theta \, d\phi, \quad (4.1)$$

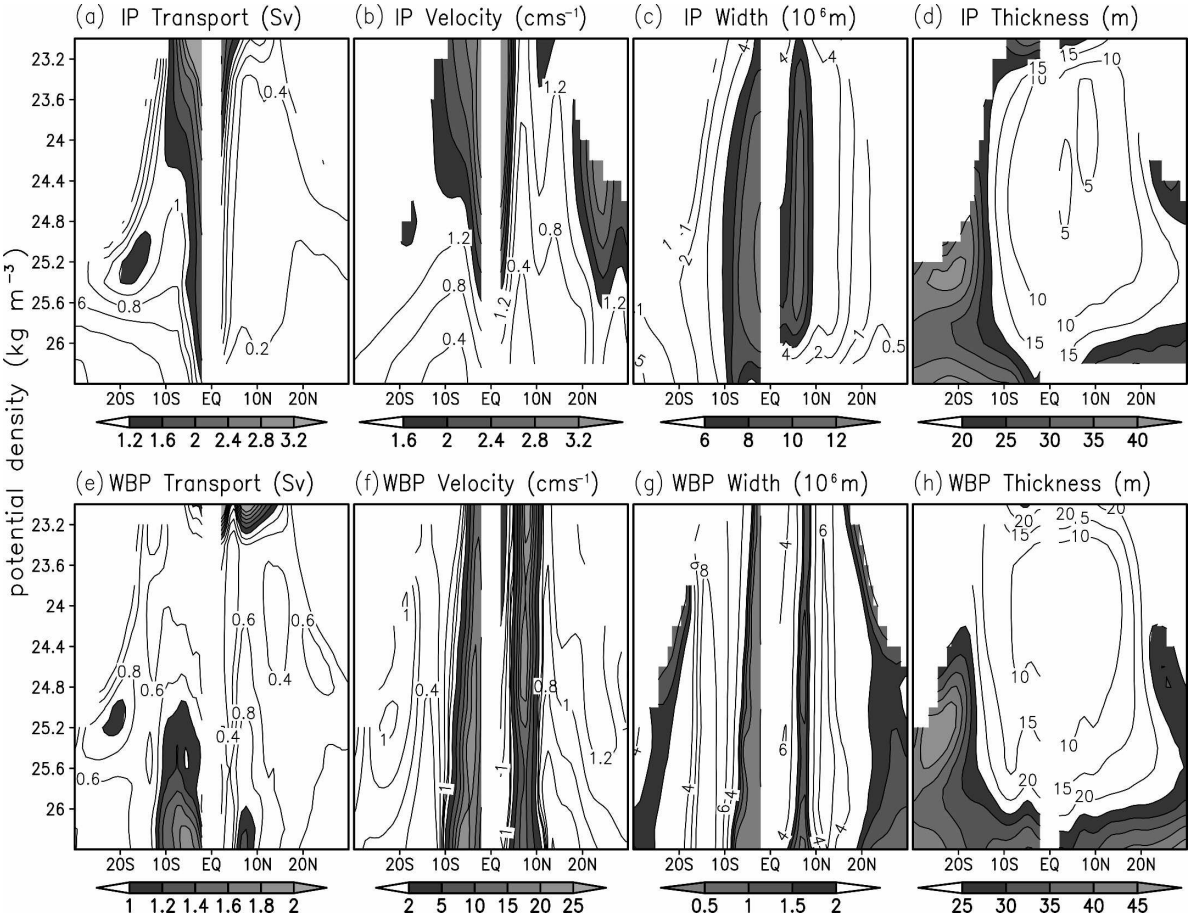

FIG. 2. Climatological-mean circulation (with 0.2-σ_θ resolution) for (top) interior pathways (IPs) and for (bottom) western boundary pathways (WBPs): (a), (e) volume transport; (b), (f) zonal-averaged meridional velocity; (c), (g) width of the pathway; and (d), (h) zonal-averaged layer thickness.

where ϕ and θ are longitude and latitude, v_n is meridional velocity (to draw figures expediently, we define equatorward v_n positive hereinafter), h_n is layer thickness, R is radius of the earth, ϕ_{En}/ϕ_{Wn} is eastern/western boundary of the pathway, and $n = 1, 2 \ldots, 18$ is the number of layers over density range $\sigma_\theta = 23.0$–26.4 kg m^{-3}. Hereinafter we will denote IPT for IP transport, WBPT for WBP transport, NIPT and NWBPT for the corresponding transport in the North Pacific, and SIPT and SWBPT for the South Pacific.

IPT increases greatly equatorward within the latitude band of ±6° (Fig. 2a). North of 6°N the NIPT is roughly constant on different isopycnal layers and latitudes. South of 6°S the SIPT within the upper layers increases rapidly equatorward, but transport in the lower layers increases slowly equatorward.

Note that an increase (decrease) in IPT with latitude implies a cross-isopycnal mass flux entering (leaving) these layers because there is no mass flux through lateral boundaries. However, in the outcrop areas, where the IP meets the surface, the IPT can increase (decrease) through water mass formation, a process that is quite different from diapycnal mixing in the deep ocean.

Within the 6° latitude band of the equator, the strong cross-isopycnal flux is closely linked to the "tropical cell." According to the definition, the tropical cell is a shallow meridional overturning circulation in the equatorial regime, induced by the poleward mass transport in the Ekman layer and the equatorward compensating return flow in the subsurface layers (McPhaden 1984; Johnson and Luther 1994; Lu et al. 1998). The existence of the tropical cell can be seen clearly from the zonal-averaged meridional velocity (Fig. 2b)

$$[v_n] = \frac{1}{\phi_{En} - \phi_{Wn}} \int_{\phi_{Wn}}^{\phi_{En}} v_n(\phi, \theta)\, d\phi.$$

The cross-isopycnal flux at low latitudes depends on the width of the IP. The SIP covers most of the equatorial Pacific; however, the NIP is quite narrow and

covers a small portion of the equatorial Pacific only (Fig. 1). As a result, at low latitudes the cross-isopycnal flux in the South Pacific is much stronger than that in the North Pacific (Fig. 2a).

In the subtropical North Pacific there is a local transport maximum centered at the $\sigma_\theta = 24.4$ kg m^{-3} outcrop area seemingly associated with strong subduction, where the zonal-averaged meridional velocity $[v_n]$ is relatively faster and the zonal-averaged layer thickness

$$[h_n] = \frac{1}{\phi_{En} - \phi_{Wn}} \int_{\phi_{Wn}}^{\phi_{En}} h_n(\phi, \theta)\, d\phi$$

is thicker (Fig. 2d). In the subtropical South Pacific there is a local transport maximum centered at $\sigma_\theta = 25.2$ kg m^{-3} that is not directly linked to outcropping, and $[h_n]$ is much thicker there (Fig. 2d). Thus, this transport maximum may be created through a strong cross-isopycnal flux.

Generally, $[v_n]$ slows down with the depth (Fig. 2b), the SIP monotonously widens equatorward, and the NIP is widest at around 7°N (Fig. 2c).

Apart from the uppermost and deep layers, the zonal-averaged layer thickness $[h_n]$ becomes thinner equatorward (Fig. 2d), reflecting the characteristics of the planetary potential vorticity conservation ($q_n = f/h_n = \text{const}$, where $f = 2\Omega \sin\theta$). However, layer thickness in the South Pacific is thicker than the North Pacific, reflecting the difference in background stratification.

Subtropics dynamic processes in the WBP are similar to the IP; thus, characteristics of transport, $[v_n]$, width, and $[h_n]$ of WBP are similar to that of IP (Figs. 2e–h). At low latitudes the WBPT maxima appear in the upper and deep layers, which are mainly determined by their thickness and velocity (Figs. 2e,f,h).

The patterns of the width and $[v_n]$ of WBP clearly indicate locations of the LLWBC (Figs. 2f and 2g). The SWBP is confined to 4°S in the uppermost layer; however, it expands with depth and extends to 9°S on the deepest layer. The NWBP is mainly limited between 6° and 9°N on all isopycnal surfaces. This means that the LLWBC in the South Pacific penetrates to an equatorial region, maintaining its jetlike form, but the LLWBC in the North Pacific loses its jetlike characteristic before entering the equatorial region. We can also see that in the South Pacific the $[v_n]$ maximum of the LLWBC appears in the deep layer, while in the North Pacific it appears in the upper layer.

5. A concise description of transport through pathways

As discussed by Huang and Wang (2001), a simple barotropic index can be used to describe the IP clearly. The situation for the baroclinic circulation is more complicated, but a similar tool can be introduced.

For a steady flow with weak friction in the ocean interior, regardless of whether there are cross-isopycnal fluxes, potential vorticity conservation is reduced to

$$\nabla \cdot [\mathbf{u}_n h_n q_n] = 0 \quad \text{or} \quad \nabla \cdot [\mathbf{u}_n f] = 0, \tag{5.1}$$

where $\mathbf{u}_n$ is the horizontal velocity in the nth layer [Pedlosky 1996, 177–187, (4.3.17) and (4.3.4)]. Equation (5.1) can be seen as a direct result of geostrophic balance on isopycnal surfaces.

Equation (5.1) allows us to introduce a virtual streamfunction ψ_n:

$$u_n \sin\theta = -\frac{\partial \psi_n}{R \partial \theta} \quad \text{and} \quad v_n \sin\theta = \frac{\partial \psi_n}{R \cos\theta \partial \phi}. \tag{5.2a,b}$$

A zonal integrating of (5.2b) leads to

$$\psi_n(\phi, \theta) - \psi_n(\phi_0, \theta) = \int_{\phi_0}^{\phi} v_n R \sin\theta \cos\theta\, d\phi. \tag{5.3}$$

If $\phi(\theta)$ and $\phi_0(\theta)$ are streamlines, the integral on the right-hand side of (5.3) should be a constant. In particular, if we choose the western and eastern boundaries of the pathway as such streamlines: $\phi(\theta) = \phi_{Wn}(\theta)$ and $\phi_0(\theta) = \phi_{En}(\theta)$, then (5.3) leads to

$$\psi_n(\phi_{En}, \theta) - \psi_n(\phi_{Wn}, \theta) = \int_{\phi_{Wn}(\theta)}^{\phi_{En}(\theta)} v_n(\phi, \theta) \sin\theta R \cos\theta\, d\phi = \text{const}. \tag{5.4}$$

Thus, both IPT per unit thickness and WBPT per unit thickness satisfy

$$\int_{\phi_{Wn}(\theta)}^{\phi_{En}(\theta)} v_n(\phi, \theta) R \cos\theta\, d\phi = \frac{\text{const}}{\sin\theta}. \tag{5.5}$$

Therefore, IPT (WBPT) per unit thickness should have a functional form

$$F_n(\theta) = \frac{\text{const}(n)}{\sin\theta}.$$

Since velocity field obtained from the model or oceans does not satisfy Eq. (5.1) exactly, IPT per unit thickness and WBPT per unit thickness satisfy (5.5) approximately.

It is readily seen from Fig. 3 that away from the equator and the western boundary and subduction area, IPT per unit thickness and WBPT per unit thickness are approximately the functional relation $F_n(\theta)$.

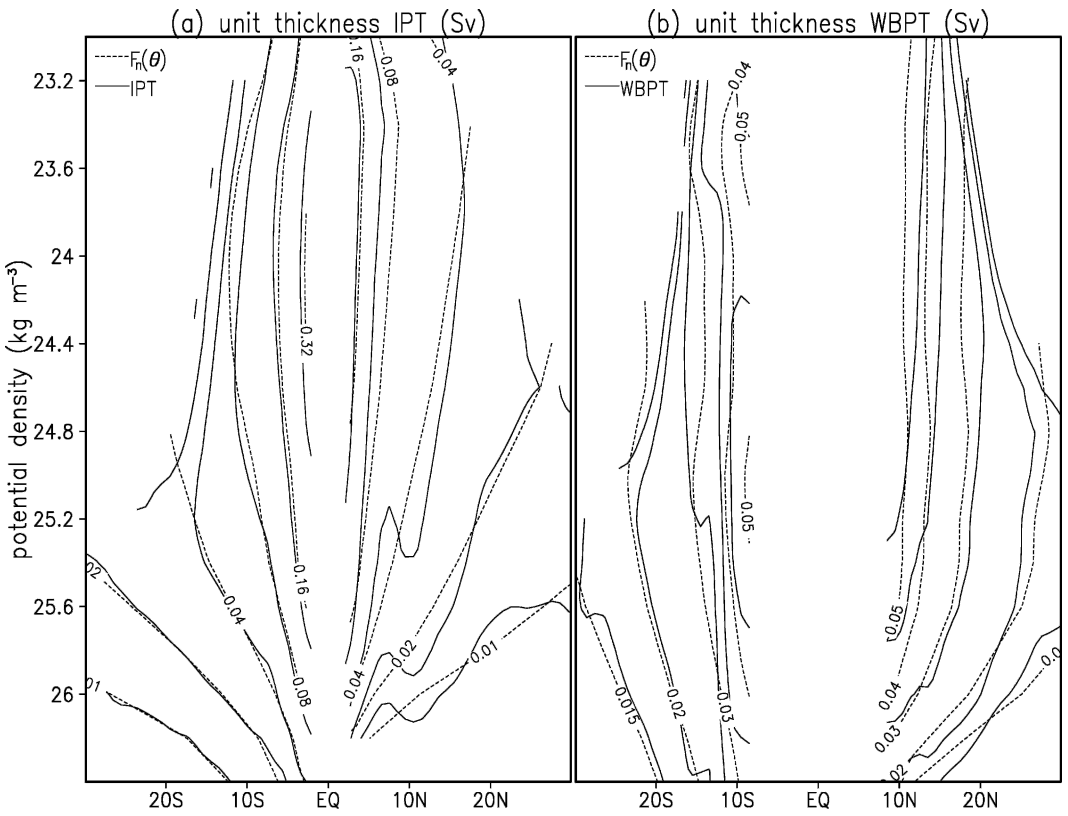

FIG. 3. Climatological-mean interior pathway transport (IPT) per unit thickness and western boundary pathway transports (WBPT) per unit thickness (solid lines); dotted lines indicate $F_n(\theta) = \text{const}(n)/\sin\theta$ (θ is the latitude).

Thus, in midocean, IPT (WBPT) per unit thickness multiplied by $\sin\theta$ is approximately constant.

By definition, flow trajectories should follow contours of the virtual streamfunction, and a comparison on $\sigma_\theta = 25.0$ kg m^{-3} is shown in Fig. 4. They are close to each other, except in the equatorial region and western boundary.

Figure 4 also gives potential vorticity and it shows that the PV,

$$q_n = \frac{\Delta\rho}{\rho}\frac{f}{h_n},$$

is not perfectly conserved along streamlines and the potential vorticity barrier under the ITCZ from our analysis is somewhat weaker than that of Johnson and McPhaden (1999), implying that SODA data may give a main thermocline thicker than observations.

From Fig. 3 and Fig. 4 we can see that Eq. (5.5) provides a concise description of the meridional dependency of IPT per unit thickness and WBPT per unit thickness in midocean.

According to Eq. (5.5), transport per unit thickness through these pathways varies with the latitude in proportion to $1/\sin\theta$. Thus, in approaching the equatorial region, IPT per unit thickness is significantly enhanced, implying either a faster meridional velocity or a wider channel. There may be two mechanisms at work. First, when approaching the equator, the layer must be compressed to accelerate the velocity and must cover a wider range in the zonal direction; second, cross-isopycnal flux can provide additional meridional mass transport.

From Fig. 2a it is seen that the first mechanism may work in deep layers in the subtropical South Pacific and subtropical North Pacific because the meridional mass transports are uniform in latitude. However, in middle and upper layers in the subtropical South Pacific cross-isopycnal flux is an important factor. At low latitudes in both hemispheres cross-isopycnal flux is needed to satisfy Eq. (5.5). This characteristic indicates that the dynamics to maintain a pathway are quite different between low latitudes and the subtropics. In the subtropical North Pacific, isopycnal layer compression itself can make a wider pathway equatorward. However, in order for the pathway to reach low latitudes more cross-

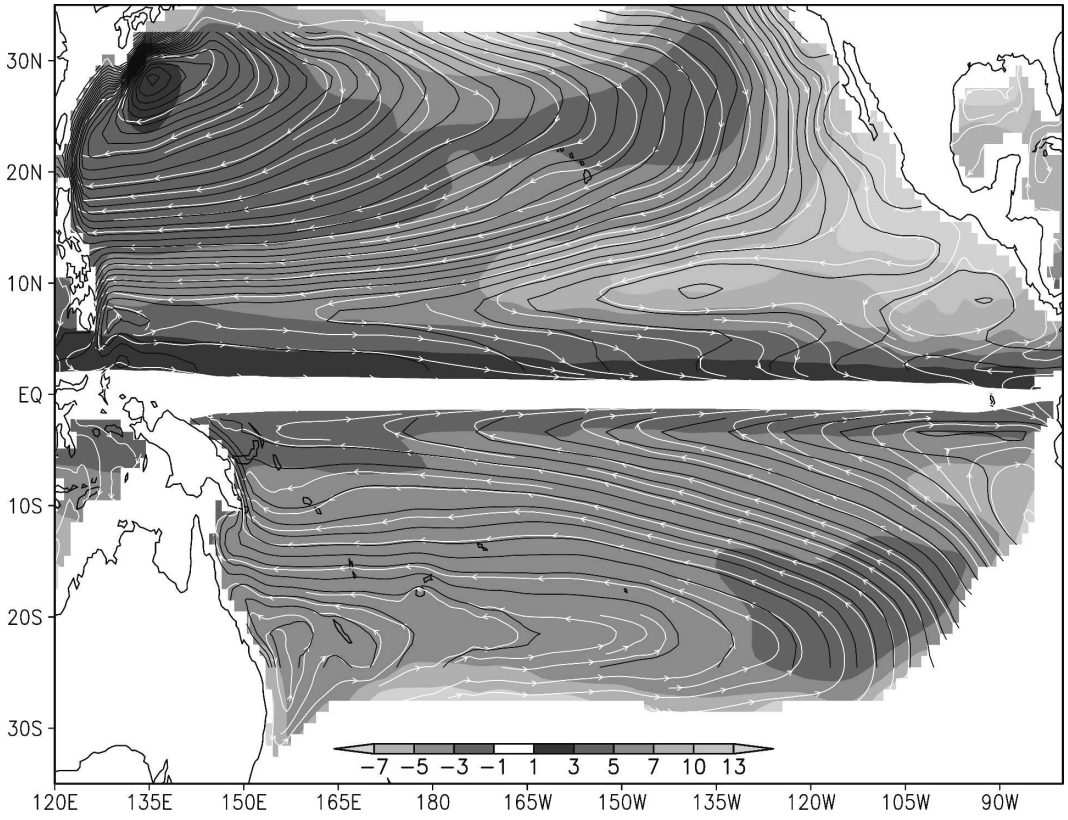

FIG. 4. Climatological-mean virtual streamfunction (black lines) and streamlines (white lines) on $\sigma_\theta = 25.0$ kg m^{-3}. The gray shades indicate potential vorticity, $q = p^{-1}\Delta pf/\Delta h$ (10^{-10} m^{-1} s^{-1}), where Δh is the layer thickness.

isopycnal flux is needed for every layer there. Our analysis indicates that at higher latitudes Eq. (5.5) is more closely satisfied than at lower latitudes; thus, transport per unit thickness at lower latitudes may be the main factor regulating the pathway.

For the climatological-mean state, wind stress plays an important role in regulating the local transport per unit thickness through two ways. First, the wind stress–induced vertical velocity gives rise to compression (or stretching) of planetary vortex filaments, which is important in the subtropics. Second, easterly wind stress produces poleward mass transports in the Ekman layer and induces an equatorward-compensating return flow in the subsurface layers that is important at lower latitudes.

Since wind stress also affects transport in subsurface layers, we should investigate the relation between wind stress and the vertical-integrated transport. In the following discussion we define the vertical-integrated ($\sigma_\theta = 23.0$–26.4 kg m^{-3}) transport: sumIPT(θ) $= \Sigma_{n=1}^{18}$ IPT$_n(\theta)$, sumWBPT(θ) $= \Sigma_{n=1}^{18}$ WBPT$_n(\theta)$ and the equatorward transport of the geostrophic flow induced by wind stress (from SODA): windIPT(θ) $= \int_{\phi_W^I}^{\phi_E^I} V_G(\phi, \theta)R\cos\theta\, d\phi$, windWBPT($\theta$) $= \int_{\phi_W^W}^{\phi_E^W} V_G(\phi, \theta)R\cos\theta\, d\phi$, where

$$V_G = \frac{1}{\beta}\,\mathrm{curl}\left(\frac{\boldsymbol{\tau}}{\rho_0}\right) + \frac{\tau_\phi}{\rho_0 f}$$

(define positive for equatorward flow $V_G > 0$), $\boldsymbol{\tau}$ is wind stress, τ_ϕ is the zonal component of $\boldsymbol{\tau}$, $\beta = 2\Omega\cos\theta/R$, R is the earth's radius, and ϕ_W^I and ϕ_E^I (ϕ_W^W and ϕ_E^W) are the western and eastern boundaries of IP (WBP) on $\sigma_\theta = 25.4$ kg m^{-3}. The following notations for the vertical-integrated transport are used hereinafter: sumIPT (sumWBPT) for the North Pacific are NsumIPT (NsumWBPT) and that for the South Pacific are SsumIPT (SsumWBPT).

(From Fig. 11a in section 6, we can see that V_G matches the vertical-integrated transport rather closely in midocean. In the subtropical North Pacific the equatorward transport is larger than that in the subtropical South Pacific; however, near 7°N the equatorward transport is reduced greatly and there is no similar "choke" latitude in the South Pacific. It can be expected that NsumIPT should be less than SsumIPT.)

As shown in Fig. 5, beyond ±3° (±9°) sumIPT

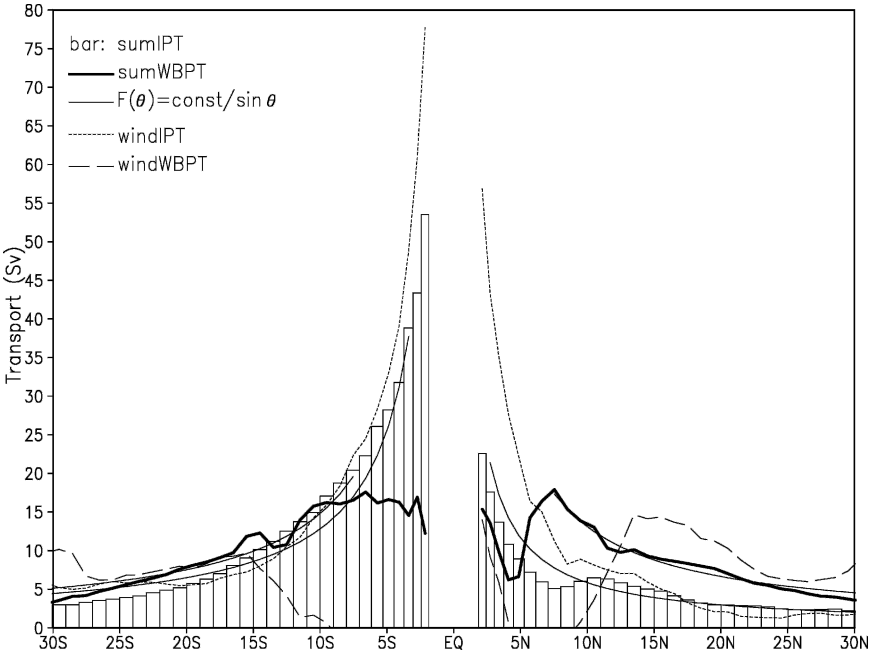

FIG. 5. Climatological-mean vertically integrated volume transports. The solid lines indicate $F(\theta)$ = const/sinθ, bars indicate sumIPT$(\theta) = \Sigma_{n=1}^{18}$ IPT$_n(\theta)$, and thick lines depict sumWBPT$(\theta) = \Sigma_{n=1}^{18}$ WBPT$_n(\theta)$. The dotted lines indicate the wind-induced equatorward transport of the geostrophic flow through the IP: windIPT$(\theta) = \int_{\phi_W^I}^{\phi_E^I} V_G(\phi, \theta) R \cos\theta \, d\phi$, and dashed line for the wind-induced geostrophic flow through the WBP, windWBPT$(\theta) = \int_{\phi_W^W}^{\phi_E^W} V_G(\phi, \theta) R \cos\theta \, d\phi$, where $V_G = \beta^{-1}\text{curl}(\boldsymbol{\tau}/\rho_0) + \tau_\phi/(\rho_0 f)$ and ϕ_W^I and ϕ_E^I (ϕ_W^W and ϕ_E^W) are the western and eastern boundaries of IP (WBP) on $\sigma_\theta = 25.4$ kg m^{-3}.

(sumWBPT) satisfies the functional relation $F(\theta)$ = const/sinθ approximately. Therefore, away from the equator and western boundary the following relations are approximately valid:

$$\text{sumIPT}(\theta)\sin\theta = \text{const} \quad \text{and} \quad \textit{sumWBPT}(\theta)\sin\theta = \text{const}. \tag{5.6a,b}$$

These relations are the same as the barotropic "virtual streamfunction" discussed by Huang and Wang [2001, their Eq. (3)].

Using Eqs. (5.6a, b) we can estimate the transport at a certain latitude. For example, if $\pm 15°$ is taken as the edge of tropical regions, only 20% of sumIPT at $\pm 3°$ comes from the subtropics, while nearly one-half comes within $\pm 6°$ off the equator. (This is dictated by the facts: sin3°/sin15° $\approx$ 0.2, and sin3°/sin6° $\approx$ 0.5.) Take $\pm 9°$ as the latitudes where WBPs enter the LLWBC. Since sin9°/sin15° $\approx$ 0.6, more than 60% of sumWBPT at $\pm 9°$ comes from the subtropics. Thus, for water masses entering the equatorial region, the percentage of subtropical water coming from the WBP should be larger than that from the IP.

The sumWBPT is roughly the same in both hemispheres, but SsumIPT is larger than NsumIPT (Fig. 5). In the North Pacific the IP enters the equatorial region mostly through the passage in the eastern basin. On the other hand, in the South Pacific the IP enters the equatorial region through a basinwide passage, mostly in the central and western parts of the basin (Huang and Wang 2001). Around 5°N the sumWBPT suddenly declines 10 Sv (Sv $\equiv 10^6$ m^3 s^{-1}), indicating a flow bifurcation feeding into the ITF.

Johnson and McPhaden (1999) estimated sumIPT as 6 Sv at 8°N and 14 Sv at 8°S (see their Fig. 6c). In this study the corresponding values are 5 Sv at 8°N and 18.4 Sv at 8°S (Fig. 5). Huang and Liu (1999) estimated that the sumWBPT and sumIPT at 10°N are approximately 14 and 3 Sv, and the sumWBPT and sumIPT at 10°S are approximately 15 and 11 Sv. In this study the corresponding values at 10°N are 14 and 5.3 Sv, and at 10°S the corresponding values are 16 and 15.3 Sv (Fig. 5). Despite different times used in the calculations, these results are consistent. The NCEP data used by Huang and Liu (1999) cover the period 1980–94; thus, the relatively weaker IP transports may reflect the slowdown of

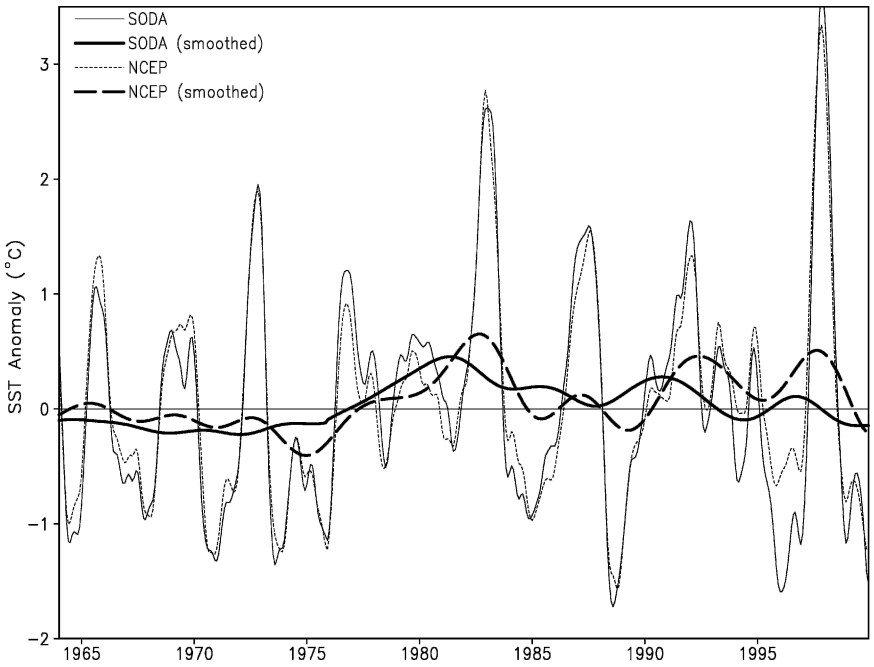

FIG. 6. SST anomalies in Niño-3: The first is obtained online from http://www.cpc.ncep.noaa.gov/data/indices/sstoi.indices (referred to as NCEP SSTa); the second is temperature at depth of 7.5 m calculated from SODA (referred to as SODA SSTa).

the meridional overturning circulation in the upper Pacific Ocean since the 1970s (McPhaden and Zhang 2002).

From Fig. 5 we can also see that windIPTs in both hemispheres increase equatorward. In the subtropics windIPTs are of the same order as sumIPTs. However, at low latitudes windIPTs are much larger than sumIPTs, especially in the North Pacific where windIPT is about 2 times sumIPT. Thus, using windIPT to estimate sumIPT at low latitudes may exaggerate the results [note we define the IP (WBP) on $\sigma_\theta = 25.4$ kg m^{-3} as the pathway of windIPT (windWBPT)].

In the subtropics windWBPTs increase equatorward and are of the same order as sumWBPTs. However, within the Tropics (around 15°S and 13°N) the windWBPTs decrease greatly; furthermore, they diminish over the latitudinal band of the LLWBCs. Thus, within Tropics changes in the sumWBPTs cannot be interpreted in terms of windWBP. However, in the equatorial North Pacific, the windWBP is consistent with sumWBPT again since the water has left the LLWBC there.

Results discussed above suggest that for a pathway in midocean its width and velocity in individual layers should satisfy Eq. (5.5), and its vertically integrated transport should satisfy Eq. (5.6). Since these restrictions can be satisfied easier in subtropics than in low latitudes, transport in the subtropics seems to play a passive role in the constitution of the pathway; that is, the pathway is primarily set by dynamical processes at low latitudes.

6. Decadal variability

Variability of the IPT and WBPT is closely linked to decadal climate variability. Analyzing hydrographic data over the past 50 years, McPhaden and Zhang (2002) found that since the 1970s the IPT has been slowing down, causing a 25% decrease in upwelling in an equatorial strip between 9°N and 9°S. These estimates indicate that the decadal variability of the WBPT is smaller than that of the IPT. Lee and Fukumori (2003) investigated the OGCM products at ±10° and found that the IPT was weaker in the 1990s than in the 1980s. Variation of the WBPT tends to be anticorrelated to the IPT, with a magnitude smaller than the IPT.

The sea surface temperature (SST) in Niño-3 was cold during 1966–75 and after the regime shift of 1976–77 it became warmer (Fig. 6). The 1988 La Niña event interrupted this warming temporarily, but it became warmer again in the 1990s.

The decadal variability of sumIPT is similar to the SSTa at Niño-3 (Fig. 7a). The sumIPT was strong during 1966–76 and weak afterward. The weak sumIPT was broken temporarily in 1987–88 and became weak again until 1998. The decadal variability of the sumWBPT

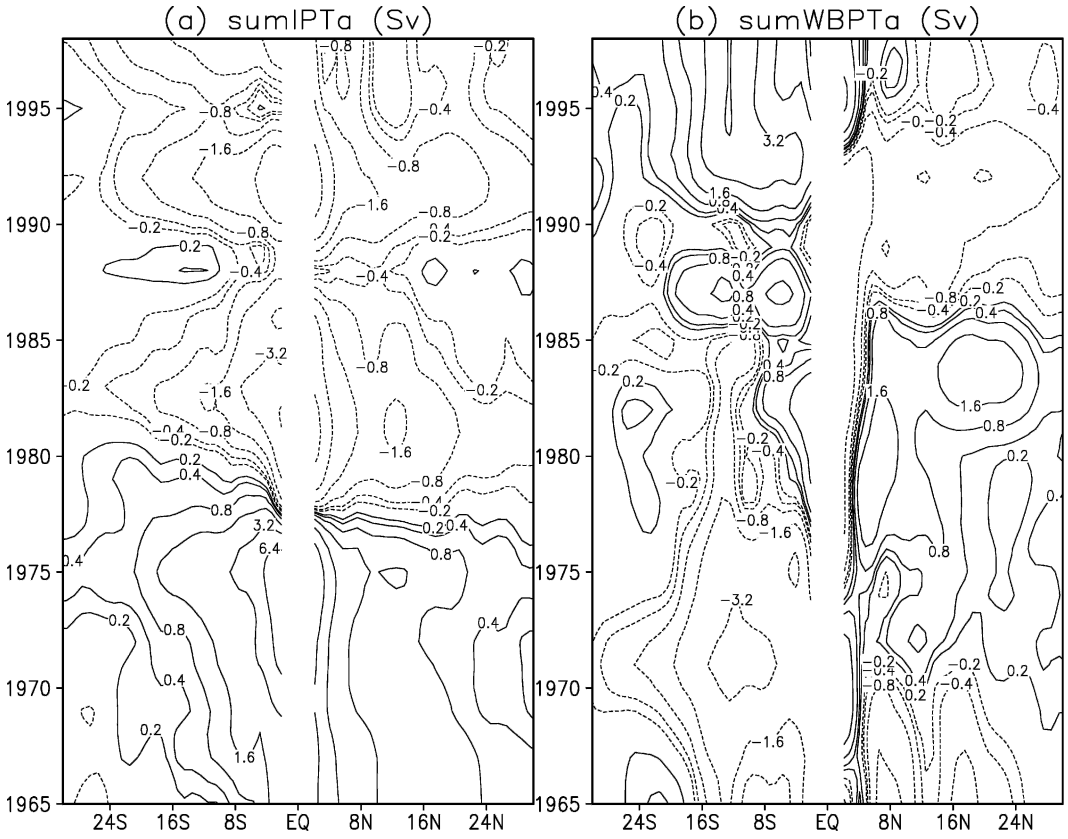

FIG. 7. Decadal variability of sumIPT and sumWBPT, with 5-yr smoothing.

is more complex than the sumIPT, even the signs in two hemispheres varied independently (Fig. 7b). Note that the phase of the decadal signal of sumIPT at 10°S lags the other one at 10°N by about 3 yr (Fig. 7a), in contrast to the opposite signs suggested by Lee and Fukumori (2003).

According to the pattern of SSTa (Fig. 6) and sumIPTa (Fig. 7a), the period from 1966 to 1998 can be divided into three subperiods: 1966–75, 1978–87, and 1990–98. During these subperiods, Eqs. (5.5) and (5.6) are approximately valid in the midocean (not shown). For each subperiod an anomaly is defined as $A_i' = A_i - \overline{A}$ and $\overline{A} = (A_1 + A_2 + A_3)/3$, where $I = 1, 2, 3$ represent three subperiods. This anomaly is further separated into three linear components, $A_i' = Va_i + Wa_i + Ha_i$: $Va_i = [v_i]'\overline{w}[\overline{h}]$, $Wa_i = w_i'[\overline{v}][\overline{h}]$ and $Ha_i = [h_i]'[\overline{v}]\overline{w}$, where w is the width of the pathway, brackets indicate zonal average in the pathway, and primes are deviations from mean.

In the subtropics IPTa is similar to *Wa*, indicating the importance of width adjustment of the pathway, while at low latitudes IPa is primarily caused by changes in velocity and layer thickness (Fig. 8).

Similar to IPT anomalies, in subtropics WBPT anomalies are mainly caused by *Wa* (Fig. 9). By comparing Fig. 9 and Fig. 8, it is seen that the variation of WBPT has a sign opposite to that of IPT for most the time (Lee and Fukumori 2003).

Unlike sumIPT, the sumIPTa in both hemispheres are of the same order, while the SsumWBPTa is somewhat larger than the NsumWBPTa during 1966–75 and 1990–98 (Fig. 10). In general, the sumWBPTa is smaller than sumIPTa, except around 15°S during 1990–98.

The windIPTa (windWBPTa) does not match sumIPTa (sumWBPTa) well (Fig. 10). In fact, they may have opposite signs at some latitudes. This fact indicates that the variability of pathway transport is not entirely determined by local wind forcing. The sumIPTa and sumWBPTa can be explained clearly by combing Figs. 10 and Fig. 11, and the latter gives the mean wind-induced meridional transport

$$V_G = \frac{1}{\beta}\,\mathrm{curl}\left(\frac{\boldsymbol{\tau}}{\rho_0}\right) + \frac{\tau_\phi}{\rho_0 f},$$

the vertically integrated (σ_θ = 23.0–26.4 kg m^{-3}) meridional transport sumT = $\Sigma_{n=1}^{18} v_n h_n$, and their anomalies. Although the basin-scale distributions of V_G and

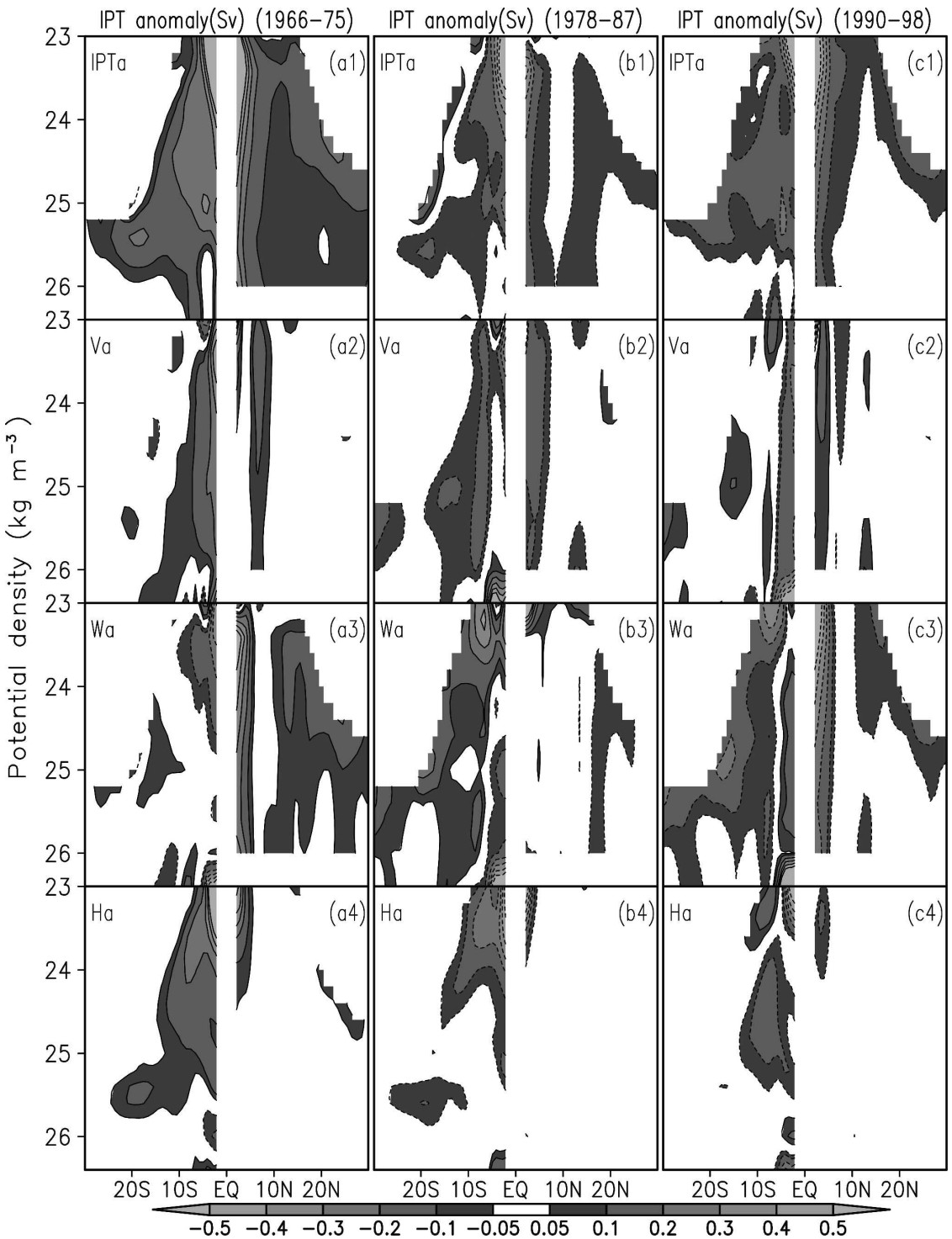

FIG. 8. (a1)–(c1) Decadal variability of IPT; (a2)–(c2) transport anomaly caused by velocity anomaly $Va = [v]'\overline{w}[\overline{h}]$; (a3)–(c3) by width anomaly $Wa = w'[\overline{v}][\overline{h}]$; and (a4)–(c4) by thickness anomaly $Ha = [h]'[\overline{v}]\overline{w}$. Angle brackets depict the zonal average over the pathway; solid contours indicate positive anomaly, and dashed contours are for negative contours.

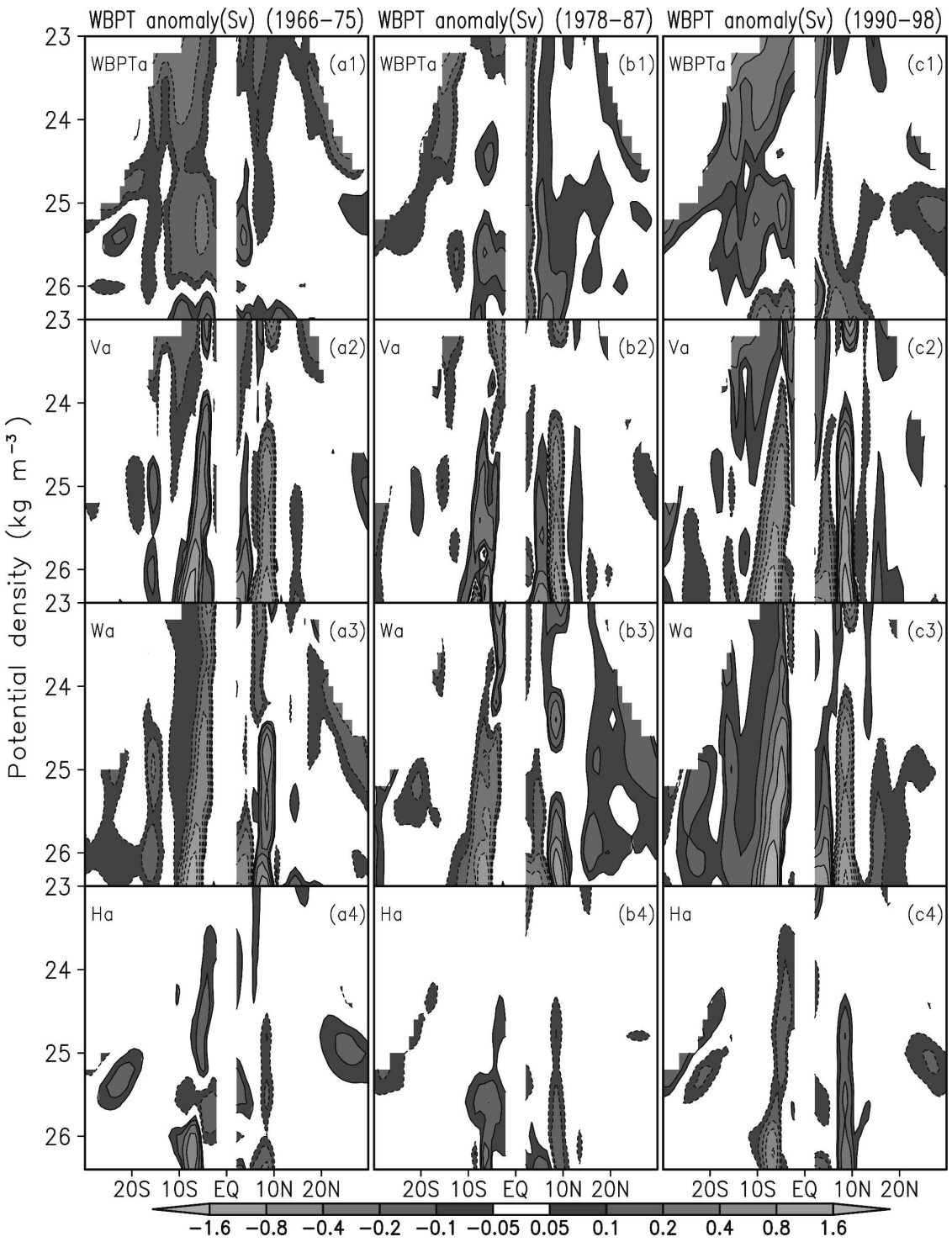

FIG. 9. Decadal variability of WBPT; see caption of Fig. 8 for the details.

sumT are similar (Fig. 11a), the variability of these two field are different (Figs. 11b–d). As compared with the V_G anomalies, the sumT anomalies appear in "wave-like" patches in a zonal direction. Nevertheless, the patterns of V_G and sumT share similar features somewhere at low latitudes.

During the period 1966–75 both V_G and sumT were stronger over a large zonal range of the low latitudes

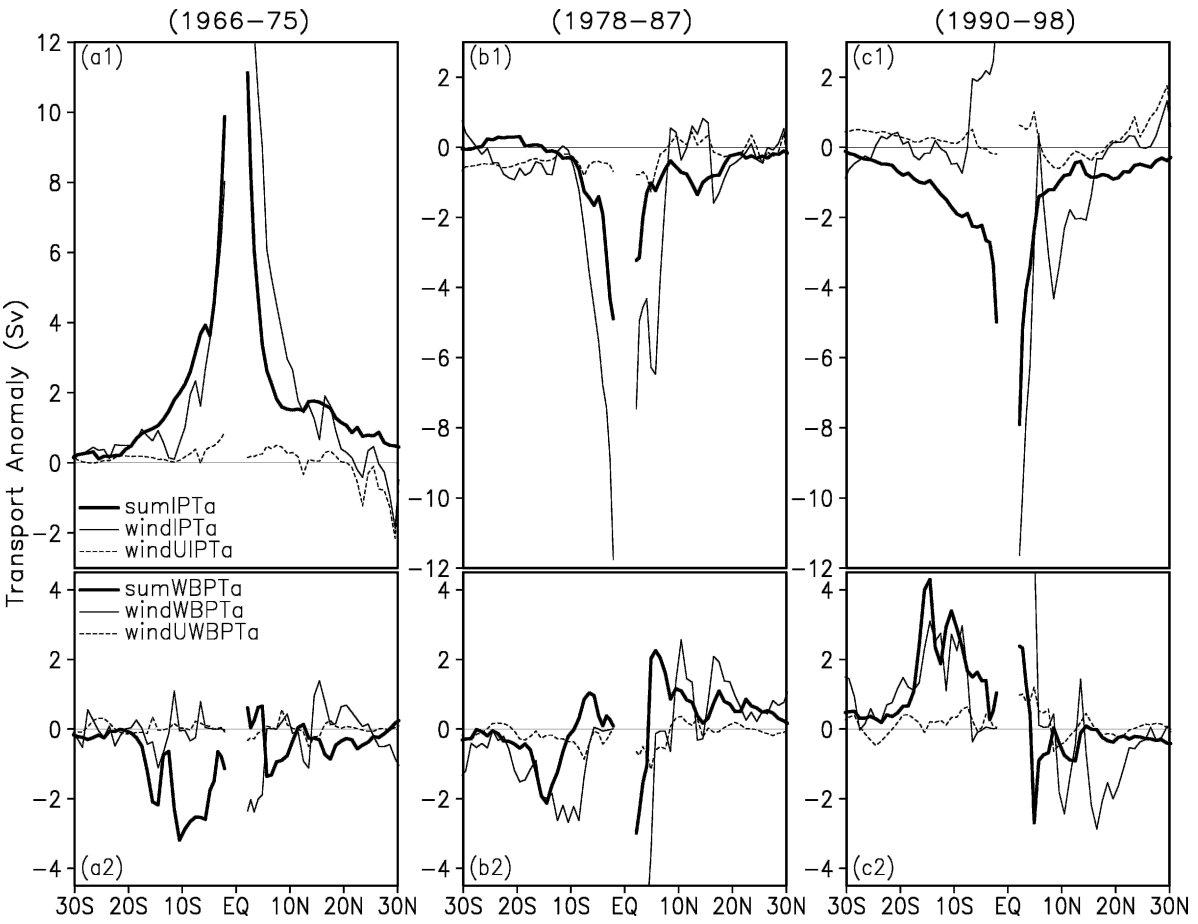

FIG. 10. The vertical-integrated transport anomalies sumIPTa (sumWBPTa) and the wind stress–induced transport anomalies windIPTa, (windWBPTa), and anomalies per unit width of the windIPT (windWBPT): windUIPTa (windUWBPTa).

(Fig. 11b). The strong V_G induced a speedup and layer thickening of the IPs at low latitudes (Figs. 8a2,a4). To satisfy Eq. (5.5), the width of the IP should be adjusted accordingly along the latitude, causing changes in the widths with latitude (Fig. 8a3). From Fig. 10a1 we can see that in the South Pacific windUIPTa is positive and the largest anomaly is near the equator. Thus, along the IP the wind stress favors a more equatorward transport, especially near the equator. In the North Pacific windUIPTa is positive at low latitudes and negative in the subtropics, and the positive sumIPTa in the subtropics is mainly due to a positive width anomaly of a pathway there (Fig. 8a3). Thus, the positive sumIPTa during 1966–75 is mainly caused by the wind stress anomaly at low latitudes.

During 1978–87 near the equatorial North Pacific and within 30°S over most of the central-eastern part of the South Pacific, both V_G and sumT were weaker (Fig. 11c). The weak V_G gave rise to thin layers and a slow motion through the IPs at the equatorial North Pacific and within 30°S of the South Pacific (Figs. 8b2,b4). In the North Pacific the windUIPT is much weaker near the equator and is relatively smaller in the subtropics, as the negative NsumIPTa in the subtropics is mainly a result of the pathway's narrowness (Fig. 8b3). Thus, we can explain that the negative NsumIPTa during 1978–87 was mainly caused by the wind force near the equator. The negative SsumIPTa is the result of the negative wind force along the SIP.

From Fig. 11d we can see that during 1990–98 in the western basin of the South Pacific low latitude, both V_G and sumT were negative, and near the central-eastern equator of the North Pacific both V_G and sumT are positive; however, there was a WS–EN band between 5° and 15°N in the central basin where both V_G and sumT were negative. Such wind stress gave rise to thinner layers and a slow motion through SIPs at low latitudes, and NIP was slow around 8°N, but was faster near the equator (Fig. 8c2,c3). From Fig. 10c1 it is readily seen that in the South Pacific all of the

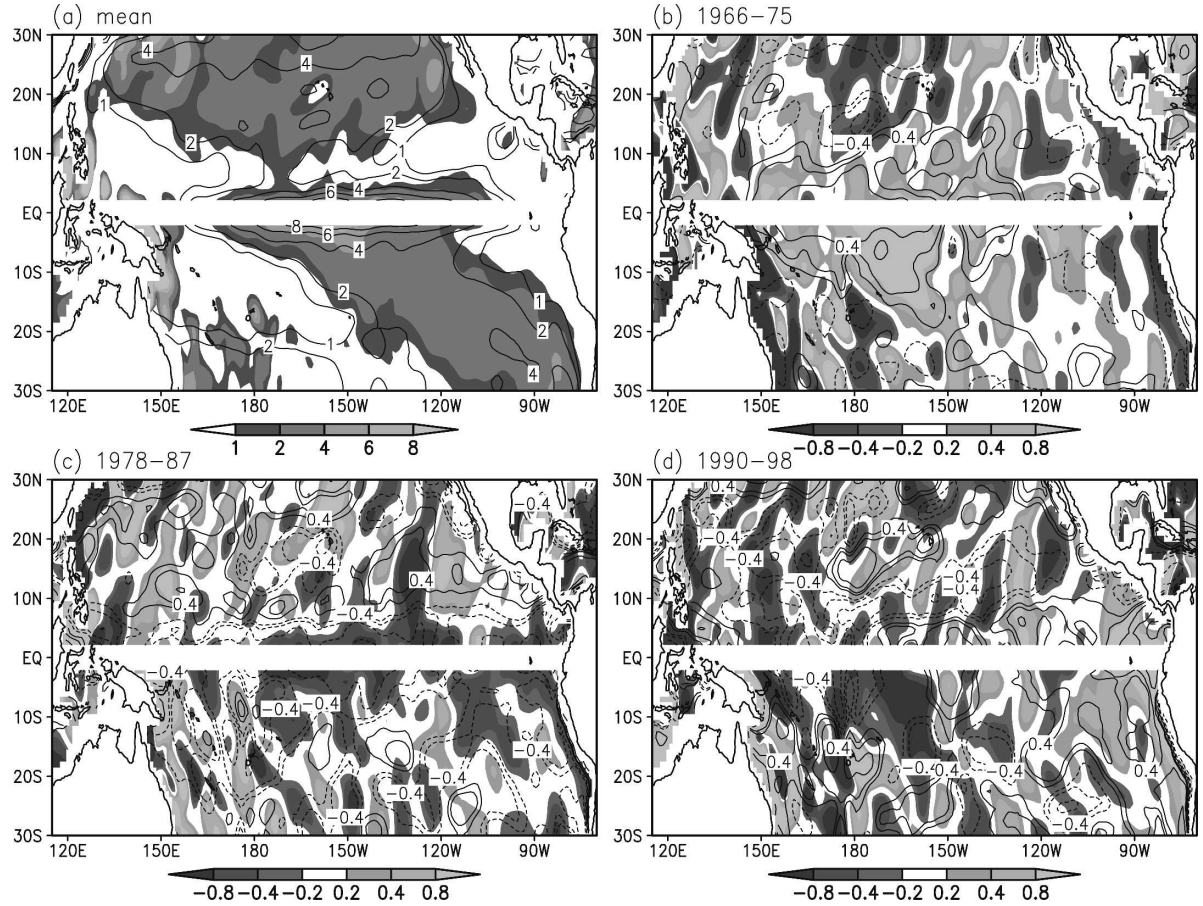

FIG. 11. The wind-induced transport $V_G = \beta^{-1}\text{curl}(\boldsymbol{\tau}/\rho_0) + \tau_\phi/(\rho_0 f)$ (contours, $\text{m}^2\,\text{s}^{-1}$) and the vertical-integrated (over density range σ_θ = 23.0–26.4 kg m^{-3}) transport sumT = $\Sigma_{n=1}^{18} v_n h_n$ (shaded area, $\text{m}^2\,\text{s}^{-1}$): (a) mean state (the equatorward transport only) and (b)–(d) anomaly over different periods.

windUIPTa are positive, except near the equator. In the North Pacific the windUIPTa is negative between 6° and 15°N and positive at other latitudes. The negative NsumIPTa during 1990–98 can be attributed primarily to the wind force around the "choke latitude" (Huang and Wang 2001). According to Eqs. (5.5) and (5.6), the NIPs adjust their widths near the equator and subtropics (Fig. 8c3). It seems difficult to explain the weak SIPT by using the negative windUIPTa near the equator because it is too small (Fig. 10c1). However, from Fig. 11d and Fig. 8c, we can explain that the weak wind force in the low-latitude western basin of the South Pacific weakens the SIPT near the equator; thus, to satisfy Eqs. (5.5) and (5.6) the width of the SIP is reduced at other latitudes.

Eight degrees North (15°S) off the equator NsumWBPTa (SsumWBPTa) increases or decreases equatorward monotonously (Figs. 10a2,b2,c2) since NsumWBPT (SsumWBPT) satisfies Eq. (5.6) approximately. Most of the time sumWBPTa has a sign opposite to sumIPTa, reflecting a partial compensation. However, during 1990–98 both NsumIPT and NsumWBPT were weak. Meanwhile, weak (strong) windWBPT corresponds to weak (strong) sumWBPT within tropical latitudes in different periods.

Near the equator NsumWBPT is primarily regulated by local wind (Fig. 10) since this is the place where water is separated from the LLWBC. However, the mechanism regulating SsumWBPT near the equator is more complicated because WBP appears in a jetlike form, entering/crossing the equator and meeting water from the Northern Hemisphere.

In summary, the wind stress anomaly at low latitudes may be the primary cause of the IPT anomaly, while the role of the subtropics might be limited. For most of the time, the WBPT anomaly has a sign opposite to the IPT anomaly, reflecting compensation between the IPT and the WBPT. However, most of the time wind stress anomaly within tropical latitudes can also be used to explain the WBPT anomaly.

7. Conclusions

A method to quantify isopycnal pathways from the subtropics to the equator is proposed and tested. This method provides well-defined pathways and detailed information related to how does transport through these pathways vary with latitude and depth.

Since no mass flux is allowed through the lateral boundaries of the pathways, change of the meridional transport with latitude implies cross-isopycnal flux. Our analysis indicates that within the $\pm 6°$ latitude band of the equator, there is a strong cross-isopycnal mass flux in the IP. At latitudes 6° off the equator the cross-isopycnal mass flux in the SIP is stronger than the NIP. The SWBP passes through the LLWBC and penetrates the equatorial region, maintaining a jetlike form. However, NWBP leaves the MC around 4°N and loses its jetlike characteristic before entering the equatorial region.

In each layer contours of the virtual streamfunction serve as good approximations for streamlines, regardless of diapycnal flux. This means the zonal-integrated meridional transport per unit thickness in the pathway increases equatorward in proportion to $1/\sin\theta$. A large increase in transport near the equator implies either a stronger meridional velocity or a wider channel in the longitudinal direction.

Transport at lower latitudes is the main factor regulating the pathway. For the long-term mean state the IP is primarily controlled by wind stress at low latitudes, and the WBP is determined by wind stress at higher latitudes because the WBP enters the LLWBC at higher latitudes.

Transport through pathways has prominent decadal variability. Our results suggest that on decadal time scales the IPT anomaly may be primarily regulated by wind stress anomalies at low latitudes. The compensation between the WBPT and the IPT, and wind stress anomaly within tropical latitudes may be responsible for the WBPT anomaly.

Acknowledgments. QW was supported by The National Natural Science Foundation of China through Grants 40176003 and 40136010 and National Key Program for Developing Basic Research of China through Grants 2005CB422301. RXH was supported by the National Oceanic and Atmospheric Administration through CICOR Cooperative Agreement NA17RJ1223 and National Science Foundation through Grant OCE-0094807 to the Woods Hole Oceanographic Institution. Comments from Dr. Eric Firing and two anonymous reviewers were most helpful. QW acknowledges constructive suggestions and help from Drs. Johan Nilsson and Peter Lundberg.

REFERENCES

Blanke, B., and S. Raynaud, 1997: Kinematics of the Equatorial Undercurrent: An Eulerian and Lagrangian approach from GCM results. *J. Phys. Oceanogr.,* **27,** 1038–1053.

Carton, J. A., G. Chepurin, X. Cao, and B. S. Giese, 2000a: A simple ocean data assimilation analysis of the global upper ocean 1950–95. Part I: Method. *J. Phys. Oceanogr.,* **30,** 294–309.

——, ——, and ——, 2000b: A simple ocean data assimilation analysis of the global upper ocean 1950–95. Part II: Results. *J. Phys. Oceanogr.,* **30,** 311–326.

Fine, R. A., W. H. Peterson, and H. G. Ostlund, 1987: The penetration of tritium into the tropical Pacific. *J. Phys. Oceanogr.,* **17,** 553–564.

Huang, B., and Z. Liu, 1999: Pacific subtropical–tropical thermocline water exchange in the National Centers for Environmental Prediction ocean model. *J. Geophys. Res.,* **104,** 11 065–11 076.

Huang, R. X., and Q. Wang, 2001: Interior communication from the subtropical to the tropical oceans. *J. Phys. Oceanogr.,* **31,** 3538–3550.

Johnson, E. S., and D. S. Luther, 1994: Mean zonal momentum balance in the upper and central equatorial Pacific Ocean. *J. Geophys. Res.,* **99,** 7689–7705.

Johnson, G. C., and M. J. McPhaden, 1999: Interior pycnocline flow from the subtropical to the equatorial Pacific Ocean. *J. Phys. Oceanogr.,* **29,** 3073–3098.

Lee, T., and I. Fukumori, 2003: Interannual-to-decadal variations of tropical-subtropical exchange in the Pacific Ocean: Boundary versus interior pycnocline transports. *J. Climate,* **16,** 4022–4042.

Liu, Z., 1994: A simple model of the mass exchange between the subtropical and tropical ocean. *J. Phys. Oceanogr.,* **24,** 1153–1165.

——, and B. Huang, 1998: Why is there a tritium maximum in the central equatorial Pacific thermocline? *J. Phys. Oceanogr.,* **28,** 1527–1533.

——, S. G. H. Philander, and R. C. Pacanowski, 1994: A GCM study of the tropical–subtropical upper-ocean water exchange. *J. Phys. Oceanogr.,* **24,** 2606–2623.

Lu, P., and J. P. McCreary Jr., 1995: Influence of the ITCZ on the flow of thermocline water from the subtropical to the equatorial Pacific Ocean. *J. Phys. Oceanogr.,* **25,** 3076–3088.

——, ——, and B. A. Klinger, 1998: Meridional circulation cells and the source waters of the Pacific equatorial undercurrent. *J. Phys. Oceanogr.,* **28,** 62–84.

McCreary, J. P., and P. Lu, 1994: On the interaction between the subtropical and the equatorial oceans: The subtropical cell. *J. Phys. Oceanogr.,* **24,** 466–497.

McPhaden, M. J., 1984: On the dynamics of the equatorial subsurface countercurrents. *J. Phys. Oceanogr.,* **14,** 1216–1225.

——, and R. A. Fine, 1988: A dynamical interpretation of the tritium maximum in the central equatorial Pacific. *J. Phys. Oceanogr.,* **18,** 1454–1457.

——, and D. Zhang, 2002: Slowdown of the meridional overturning circulation in the upper Pacific Ocean. *Nature,* **415,** 603–608.

Pedlosky, J., 1996: *Ocean Circulation Theory.* Springer-Verlag, 453 pp.

Rothstein, L. M., R.-H. Zhang, A. J. Busalacchi, and D. Chen, 1998: A numerical simulation of the mean water pathways in the subtropical and tropical Pacific Ocean. *J. Phys. Oceanogr.,* **28,** 322–342.